Available online at www.sciencedirect.com

ScienceDirect

Advances in Space Research 73 (2024) 698–715

ADVANCES IN SPACE RESEARCH (a COSPAR publication)

www.elsevier.com/locate/asr

Performance evaluation for vertical TEC predictions over the East Africa and South America: IRI-2016 and IRI-2020 versions

Habtamu Marew [a,b,*], Abebech Agmas [b], Tsedal Mersha [b]

[a] Institute of Atmpospheric Physics, Czech Academy of Sciences, Prague, Czechia
[b] Department of Physics, College of Natural and Computational Sciences, Debre Tabor University, Ethiopia

Received 1 July 2023; received in revised form 18 September 2023; accepted 26 September 2023
Available online 29 September 2023

Abstract

In this paper, we evaluate and report the International Reference Ionosphere (IRI) model's vertical Total Electron Content (TEC) regional profile. Diurnal, monthly, seasonal, and storm-time characteristics of IRI estimates over the equatorial region's ionosphere are validated. We compared the vertical TEC derived from IRI-2020 and its predecessor, IRI-2016, with the GPS-TEC measurements. Results show that IRI (both versions) agrees with observed TEC during solar cycle maximum periods. Exceptionally, over Turkwel station, IRI-2020 produced double peak profiles on the March equinox, June solstice, and September equinox and overestimated with larger discrepancies. Over the other three stations, both IRI versions reproduced the seasonal averaged observed TEC with only slight time lags and discrepancies. During geomagnetically perturbed times, IRI-2020 better indicated positively enhanced GPS-TEC than IRI-2016. However, during the March 17, 2015 storm, IRI-2020 underestimated the storm-enhanced TEC over Bahir Dar station at all phases of the storm. IRI-2016 shows good performances for negative storms where lower TEC measurements are recorded.

Keywords: IRI-2020 model; GPS; Validation; Ionospheric TEC; Magnetic storm

1. Introduction

East Africa, as a developing region, is lagging behind in modern technology and demands more precise positioning and communication systems. However, in recent times, things have changing and the region is looking for better technology and good facilities. Therefore, now, as noted by Nigussie et al. (2013), having ionosphere specifications for various applications in the region needs due attention. Space weather services essentially depend on the accurate imaging of the ionosphere. The Global Positioning System (GPS) and the international Global Navigation Satellite Systems (GNSS) played the main role in bistatic plasma sensing. The information from this remote sensing enabled the ionospheric physics and space weather community to have a detailed understanding of the upper atmosphere dynamics (Galkin, 2022). Accurate characterization of the ionosphere is a very challenging task, and for this, empirical models have provided a simplified alternative way of getting the median characteristics of the ionosphere (Fejer et al., 2008; Nigussie et al., 2013; Nigussie et al., 2016; Kauristie et al., 2021). A couple of real-time and climatological ionospheric models have been developed to monitor the ionosphere. The IRI model is one of the climatological models and an internationally recognized official standard for the Earth's ionosphere. The International Standardization Organization, the European Cooperation for Space Standardization, the International Union of Radio Science, and the Committee on Space Research accepted the model as an international reference (Bilitza et al., 2022).

* Corresponding author.
E-mail address: alemu@ufa.cas.cz (H. Marew).

https://doi.org/10.1016/j.asr.2023.09.055
0273-1177/

IRI describes monthly averages of the electron density, electron temperature, ion temperature, and ion composition globally in the altitude range from 60 to 2000 km. Through time, additional parameters, including the equatorial ion drift, the occurrence probability of spread-F in the F1 layer, auroral boundaries, and the electron content from the bottom of the ionosphere to a user-specified altitude, were added to the model. Bilitza et al. (2022) reviewed enormous IRI validation studies based on scientific community requests, and the reader can obtain the new features on IRI-2020. Major updates related to total electron content (TEC) and electron density profiles include: (i) a more accurate representation of the solar activity variation of the topside electron density that is supported by in situ observations (e.g., ISIS 1, 2, Alouette 1, 2, CHAMP, GRACE, and Swarm) based on Bilitza and Xiong (2021). (ii) The D-region electron density profile is updated in IRI-2020 based on the work of Friedrich et al. (2018), which is a compilation of reliable rocket measurements and a theoretical ion-chemical model. Bilitza et al. (2022) is now a good guide for all of us (the researchers and users) interested in a deeper understanding of the model architecture and its mathematical formalism.

The majority of IRI input parameters and observations are from midlatitude regions because instruments are employed in the region more intensely than in other latitudinal regions (e.g., the African equatorial sector). Investigations on the validation of the model indicated that the model either under-estimates or over-estimates TEC and vertical drifts in equatorial and low-latitude regions (e.g., Scida et al., 2012; Ezquer et al., 2014; Tariku, 2015; Marew et al., 2019; Tariku, 2015; Tariq et al., 2019 and many more cited in these works). Large data availabilities at midlatitudes are reported, but the data from high latitudes (aurorla and polar) and low and equatorial latitudes are very low (Arikan et al., 2019). Hemispheric imbalance in datasets has a large effect on the accuracy of the model (Pignalberi, Pietrella, & Pezzopane, 2021). They also added that IRI is generally more accurate for the northern hemisphere.

Studies have been reported on the performance of IRI-2016 (e.g., Chen et al., 2020; Endeshaw, 2020; Moses et al., 2021; Ogwala et al., 2021; and Ogwala et al., 2022). For instance, Endeshaw (2020) showed that during the high solar activity years (2012–2016), the IRI-2016 overestimated the GPS-TEC. Average peak GPS-TEC at equatorial and low latitudes shows an equal magnitude in the March and September equinoxes (Ogwala et al., 2021). A related parameter with similar factors for variations is hmF2 of the F2-region ionosphere. Moses et al. (2021) compared the hmF2 of the IRI-2016 with the hmF2 derived from the Constellation Observing System for Meteorology, Ionosphere, and Climate (COSMIC) ionospheric occultation and reported that the IRI-2016 performs better during magnetically quiet conditions in both solar active and passive cycles. They also reported that the best predictions are made during the daytime. However, there are no validation works yet (to this point in time) for the latest IRI-2020 model.

This article focuses on the validation of the latest versions of the IRI model (IRI-2016 and IRI-2020), which are available on NASA's Community Coordinated Modeling Center (CCMC) website. Evaluations have been done for both quiet and disturbed (storm-time) geomagnetic conditions. GPS-TEC (observed vertical TEC) measurements are used for the validation. We analyzed the vertical TEC obtained from the equatorial latitudes in East Africa and Latin America. We analyzed one year of observations and model estimations for the stations: Sheba, Eartiria; and Bahir Dar, Ethiopia; Turkwel, Kenya; and Arequipa, Peru. Details about the stations are available below. However, measurements of magnetically disturbed days are excluded for quiet time analysis, as will be described in the next section. We compared the daily, averaged seasonal, and averaged monthly TEC obtained from the models and GPS. Hopefully, results will provide potential feedback to the IRI model working group and to the scientific community regarding regional performance, especially in the latest version, IRI-2020 performance.

2. Data and methods

2.1. Data

Four GPS stations are selected systematically based on their latitudinal and longitudinal location (i.e., stations that can represent the vast area of latitudes within a specific longitudinal sector (35^0 –40^0), East Africa; see Table 1). And, a fourth station for longitudinal assessment from Latin America. Thus, vertical TEC data are collected and processed for those stations from the UNAVCO website (https://www.unavco.org/). IRI-2016 and IRI-2020 model estimations are driven from NASA's CCMC website (https://kauai.ccmc.gsfc.nasa.gov/instantrun/iri). Kp-index data are obtained from NASA's Space Physics Data Facility via https://omniweb.gsfc.nasa.gov/. The British Geological Survey (https://www.geomag.bgs.ac.uk/) geomagnetic coordinate calculator has been used to obtain the corresponding geomagnetic coordinates of the GNSS/GPS stations.

2.2. Methods of analysis

Evaluations of the capacity of the IRI models have been done for both quiet and disturbed (storm-time) geomagnetic conditions. GPS-TEC (observed vertical TEC) measurements are used for validation. We analyzed the vertical TEC obtained from the equatorial latitudes in East Africa and Latin America. We analyzed one year of observations and model estimations for the stations mentioned above. The GPS Rinex observation and navigation files have a time resolution of 30 s. Using a GPS-TEC analysis software, observation and navigation row data are processed to obtain the required vertical TEC. The

Table 1
Locations of the GNSS/GPS stations and Data used for the study.

Stations location	Station code	Geog. Latitude	Geog. Longitude	Mag. Latitude	Mag. Longitude	Data used (quiet time)	Data used (Storm time)
Sheba, Earitria	SHEB	15.85	39.05	8.46	112.20	2012/13	2012/13 (Two events)
Bahir Dar, Ethiopia	BDMT	11.60	37.36	3.67	111.05	2016	2015 (Two events)
Turkwel, Kenya	XTBT	3.14	35.87	−5.72	109.83	2017/18	2017/18 (Two events)
Arequipa, Peru	AREQ	−16.47	−71.49	−5.61	0.50	2021	2017/18 (Two events)

GPS-TEC analysis software provides a vertical TEC measurement with a time resolution of about one minute. TEC has been extracted with a minimum elevation of 20^0.

Then, proper filtering was performed using median averaging methods to remove outliers. To compare the GPS-TEC with the IRI-2016 and IRI-2020 models, the quiet time ($Kp < 3$) observation and TEC driven from the models are grouped or arranged in diurnal, monthly, and seasonal classes. Also, two storm (Kp greater than 6) events are analyzed at each station to evaluate the models' performance during disturbed conditions in the ionosphere. IRI storm effect predictions do not show a significant difference for low latitudes from the "storm off" choice (Bilitza et al., 2022). However, they reported improvements for mid-latitude and high-latitude predictions of the storm effects. Even though reports indicate such conclusions, we preferred to include storm time comparisons between models and observed values to help or confirm the results obtained in other locations in the low latitudes. For instance, we confirmed the results reported by Bilitza et al. (2022) over Ramey (18.50°N, 292.40°E), a low latitude region presented in Fig. 4 of their article. Thus, we are not "only" comparing the performance of the two IRI versions but also observed-TEC with model-TEC. For graphics, MATLAB programming software has been used to analyze the data and plot the results.

3. Results

3.1. Performance of IRI over Sheba

In East Africa, the difference between local time (LT) and universal time (UT) is 3:00 h (e.g., 0:00 UT is 0:00 UT + 3 = 3:00 LT). To test the models' diurnal performances, six consecutive magnetically quiet days are selected systematically for each season of the year (March equinox, June solstice, September equinox, and December solstices) for better representation. A similar analysis has been done for all four stations considered in our work (Sheba, Bahir Dar, Turkwel, and Arequipa). Our analysis follows comparisons of both magnitude and phase between measurements and model predictions.

The diurnal variation of GPS-TEC (observed TEC) over Sheba and the validation of IRI-2020 and its predecessor, IRI-2016, are presented in Fig. 1. The top panel is for days 13–18/01/2013, the second panel (counting downward) for 18–23/02/2013, the third panel for 01–06/08/2012, and the last-bottom panel for 08–13/09/2012. As shown in Fig. 1 (top panel), peak hours of observed TEC occur before 12:00 UT, and the models also show similar trends (phase). On this panel, except on the last day, all depict very good estimations made by both IRI-2016 and IRI-2020 from about 03:00 to 09:00 UT. Both models and the observed values show minimum values at nearly the same time. However, there are significant discrepancies seen between IRI (both versions) and the observed TEC; of course, the error in the observed TEC itself might account for some smaller percentage. Each panel of Fig. 1 shows a different time of observed TEC peaks (e.g., the top panel shows peaks earlier before 12:00 UT; the second panel (from the top) shows peaks at about 12:00 UT; the third and fourth panels show peaks late after 12:00 UT). These features are also similar to the IRI models, with slight time shifts. And this might be due to the seasonal effects on TEC variations because the four panels represent different seasons. A more quantitative and statistical comparison is presented in Fig. 4 based on the monthly averaged TEC. In general, both IRI model versions agree with the diurnal variation of experimental TEC (over Sheba).

In Fig. 2, seasonally averaged TEC variability over Sheba for magnetically quiet days is presented. The two model versions do not show a discrepancy (they are in phase), but there are overestimations in all seasons between 02:00 UT and 12:00 UT. Both models excellently agreed with the seasonal averaged experimental TEC between 13:00 and 24:00 UT in the case of the March and September equinoxes. On the June and December solstices, IRI-2020 shows a significant amount of overestimations throughout the day, and IRI-2016 shows overestimations during the June solstice from about 01:00 to 16:00 UT.

Fig. 3 shows the monthly mean TEC (observed, IRI-2016 and IRI-2020 TECs) over Sheba, Eartria. The TEC contour plots are over a universal time versus month axis. The color bars are normalized based on the minimum (0 TECU) and maximum (60 TECU) from all three panels in Fig. 3. 0 TECU might only be seen from either observational or model estimates. Note: 0 TECU does not indicate the absence of electrons and ions above the station. Since 1

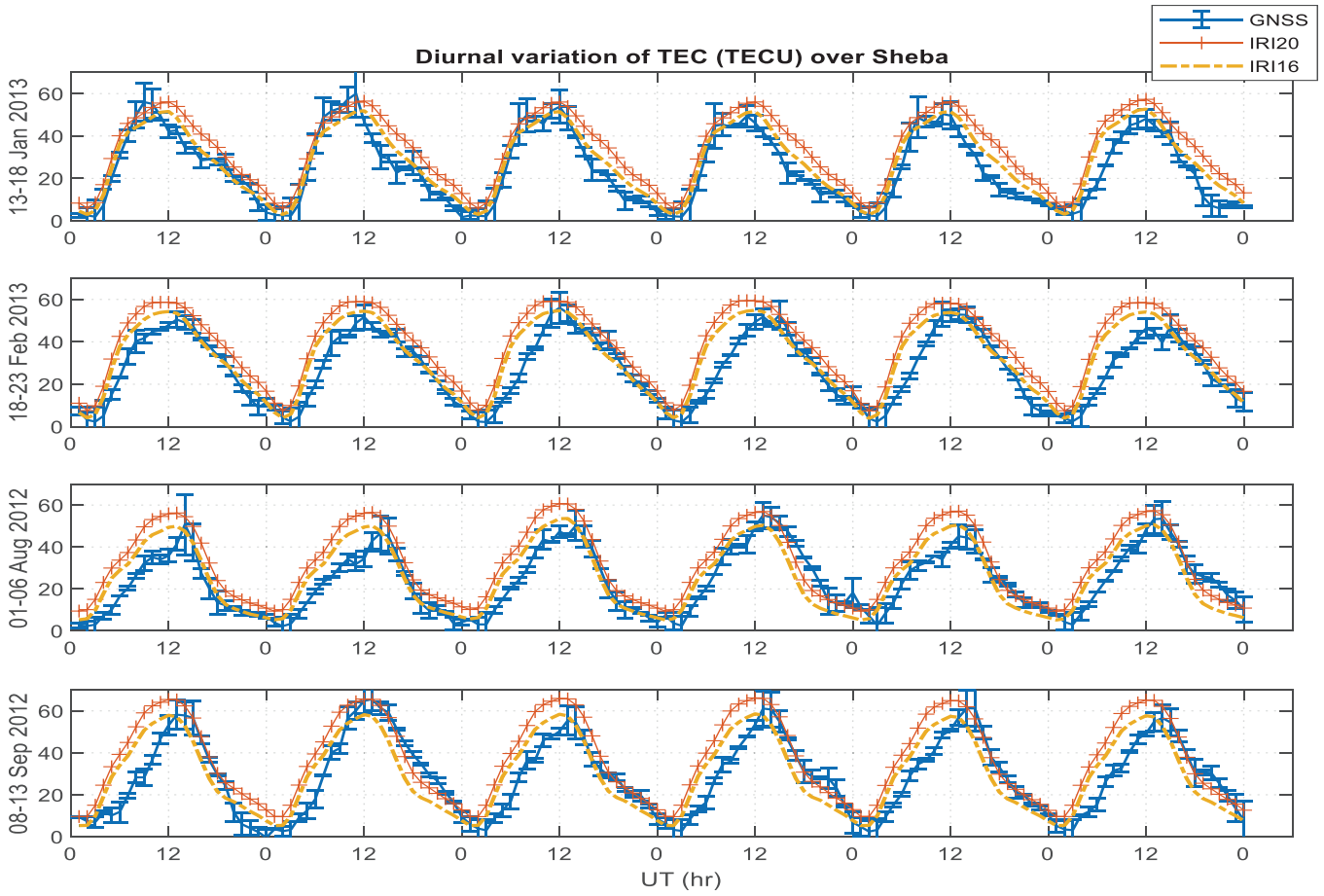

Fig. 1. Diurnal variation of vertical TEC using GPS, IRI-2016, and IRI-2020 for magnetic quiet days over Sheba. Each column represents consecutive days from different seasons. The horizontal axis is univeral time (hours), and the vertical is vertical TEC (TECU). In the legend, 'GNSS' represents TEC from a GPS receiver; 'IRI20' represents TEC from the IRI-2020 model; and 'IRI16' represents TEC from the IRI-2016 model.

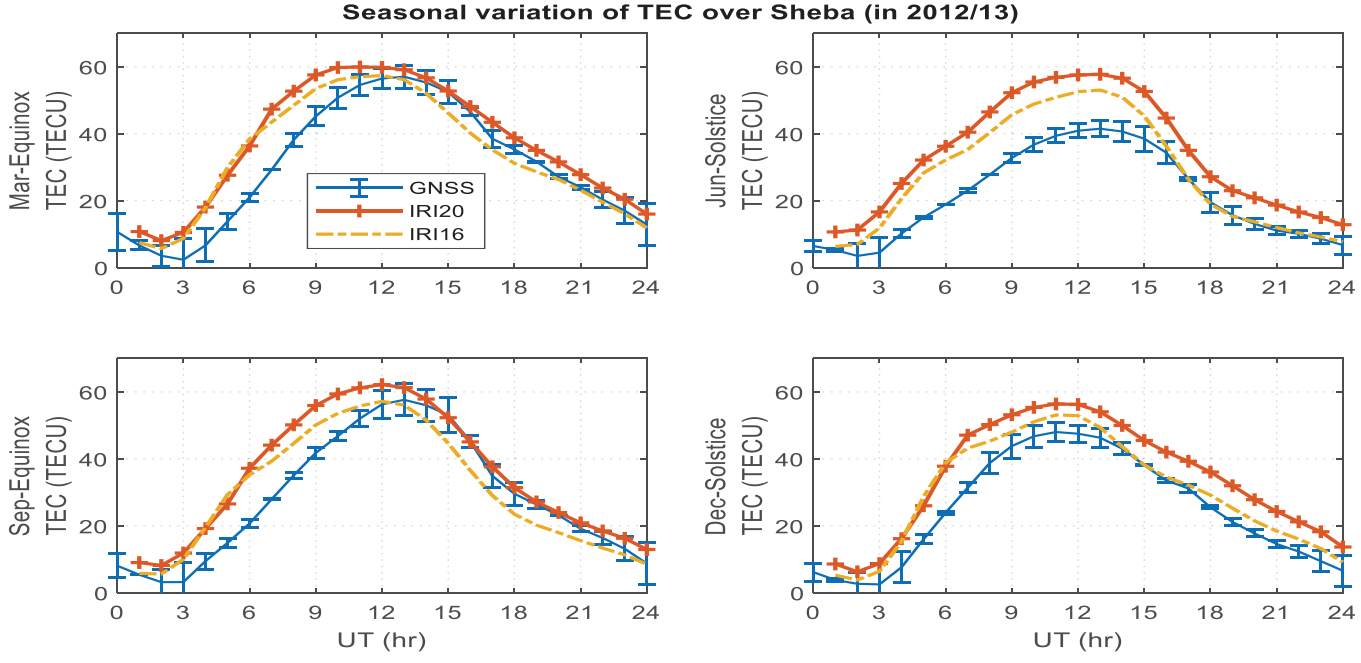

Fig. 2. Seasonal vertical TEC variations using the average of magnetic quiet days measured and model estimates over Sheba, Eritrea. Errors are calculated or estimated by subtracting the mean from each measured TEC, and error bars indicate that some mis-modeling might also be from the observations.

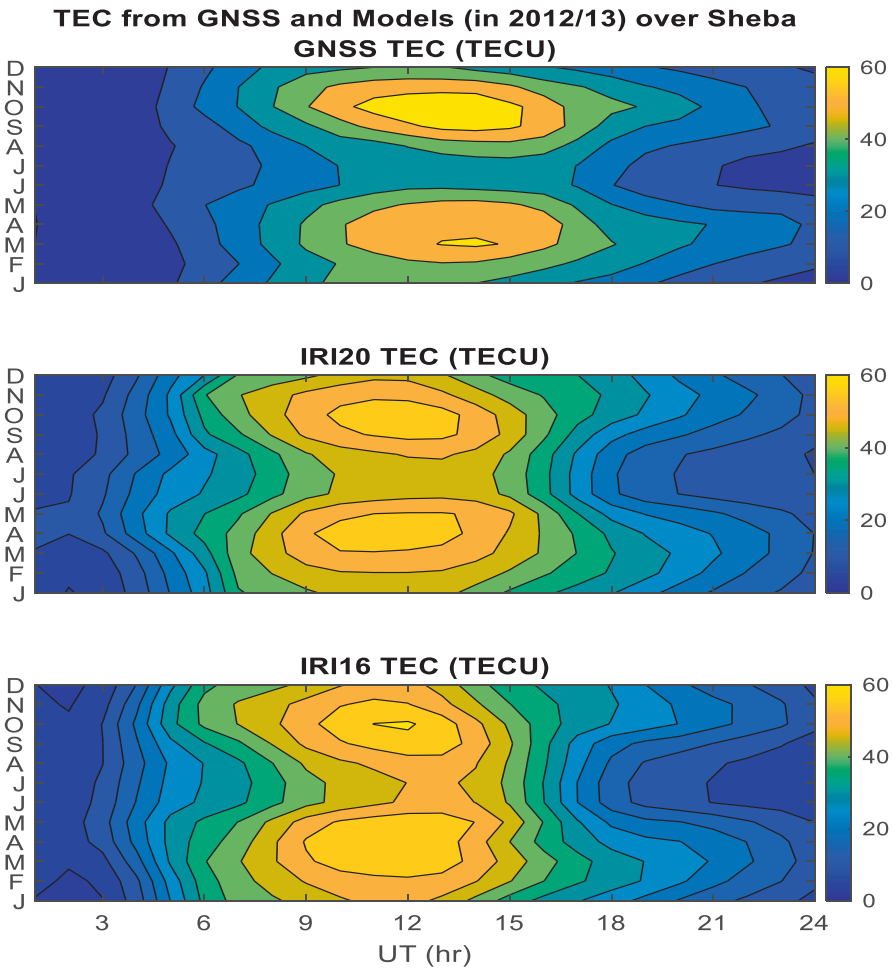

Fig. 3. Contours of the monthly mean vertical TEC during magnetic quiet times over Sheba. The horizontal axis is universal time (hours), and the vertical axis is months (January to December, bottom to top). Where the top panel is from a GPS receiver, the middle panel is from IRI-2020, and the bottom panel is from IRI-2016. Side bars on the right side are normalized to [0, 60] in TECU based on the minimum and maximum values from the three contours.

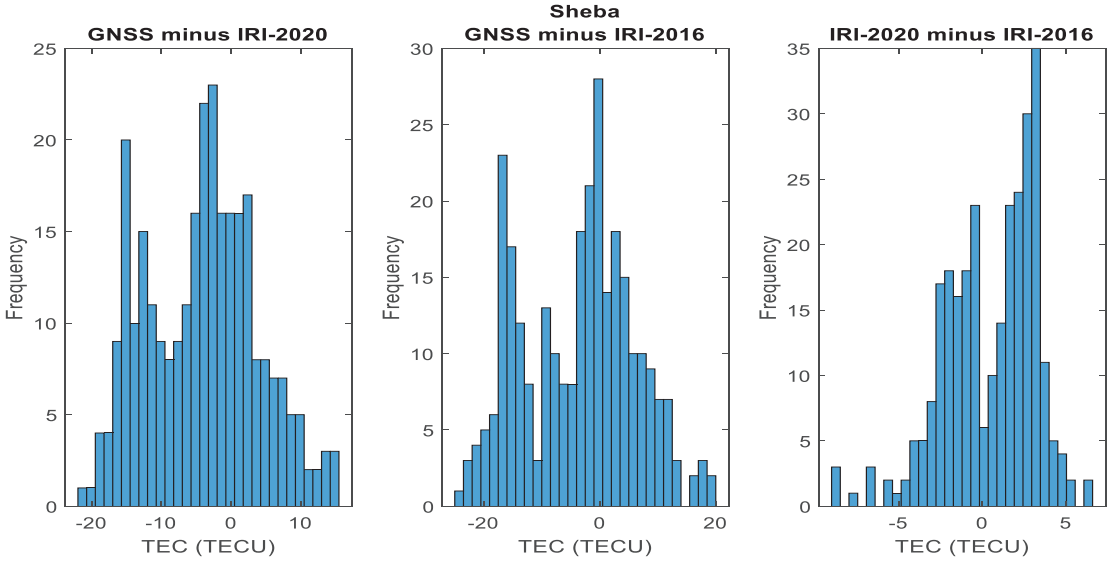

Fig. 4. A histogram of quiet-time monthly mean vertical TEC differences over Sheba (e.g., "GNSS minus IRI-2020″ represents the subtraction of IRI-2020 calculated TEC from GPS observed TEC). The vertical axis represents the number of data points for a specific calculated TEC difference (e.g., −5 TECU).

TECU = 10^{16}el/m^2 and both the TEC observed and TEC obtained from models are two decimal places after the decimal point, 0 TECU represents TEC values below 0.01 TECU. The top panel shows the monthly mean observed TEC obtained from GPS. The middle and bottom are from IRI-2020 and IRI-2016, respectively. The monthly averaged scenario shows peak values of IRI-2020 that are earlier in time than observed TEC (look at and compare the top and middle panels). From about 09:00 to 15:00 UT on the observed TEC, the peaks occur one to two hours later than the IRI-2020 peaks. With slight differences in estimation, both IRI-2020 and IRI-2016 show similar trends (no phase shifts) in monthly variations. Here, we would like to suggest that the phase shift between the observed and model data should be carefully examined and corrected.

A histogram illustration in Fig. 4 best describes the performance of the IRI models and enables the reader to understand them more statistically. This figure represents the occurrences of under- and over-estimations by the IRI models. IRI-2020 and IRI-2016 showed smaller than 5 TECU differences with the observed TEC for greater than 80% of the occasions (or 231 out of 288). 288 occasion's in simple term are a 12 × 24 averaged data points of models or/and observation. The results also indicate a significant number of cases of under- and over-estimations, some with a magnitude of about 20 TECU.

Fig. 5 is presented to show the predictions by the IRI models over Sheba during geomagnetic storms. Six consecutive days (i.e., two days from the initial main storm day and three days from the recovery phase) are selected for testing the models. A storm that occurred on July 15, 2012, has a Kp-index value of 7.0, and another that occurred on March 17, 2013 has a Kp-index of about 6.5. During the former storm event, both IRI-2020 and IRI-2016 agreed to the observed TEC during the main phase (look for the hours of days 15 and 16 of July 2012 in Fig. 5). Both versions of IRI overestimated the initial and recovery phases. The differences are too large in the recovery phase. In the latter storm event, both model versions estimated well in all phases of the storm; of course, the storm is not a strong one. Comparing the magnitude of TEC during the July 15, 2012 storm with the storm on March 17, 2013, we noticed that whenever TEC increases, the probability of the models predicting the effects also increases. Because TEC on the first panel (count down-

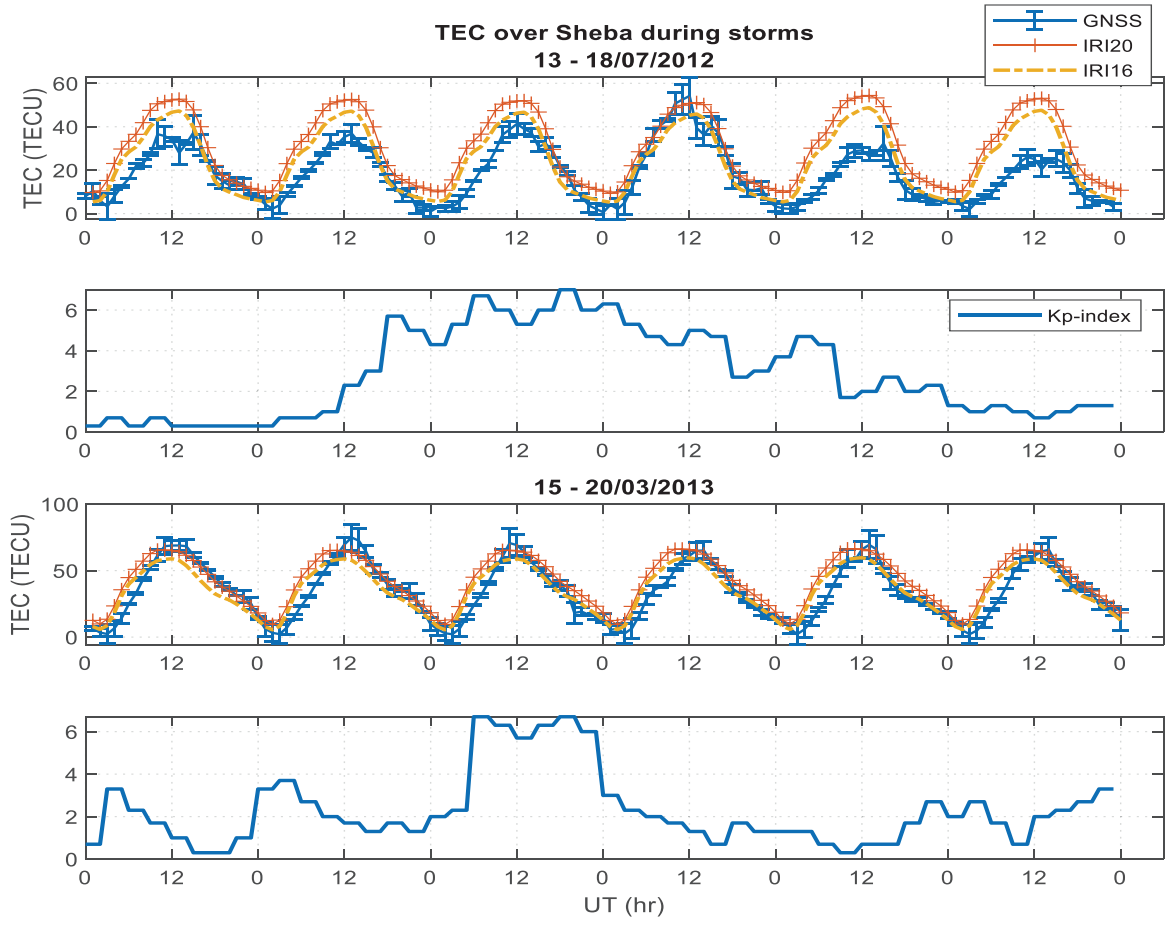

Fig. 5. Diurnal variation of vertical TEC using GPS, IRI-2016, and IRI-2020 for magnetically disturbed days over Sheba. Six consecutive days of TEC (the first two from the initial phase, the third day is a storm day, and the last three days are in the recovery phase) have been analyzed. Storms occurred on July 15, 2012, and March 17, 2013, and corresponding TEC plots are presented on the first (top) and third panels, respectively.

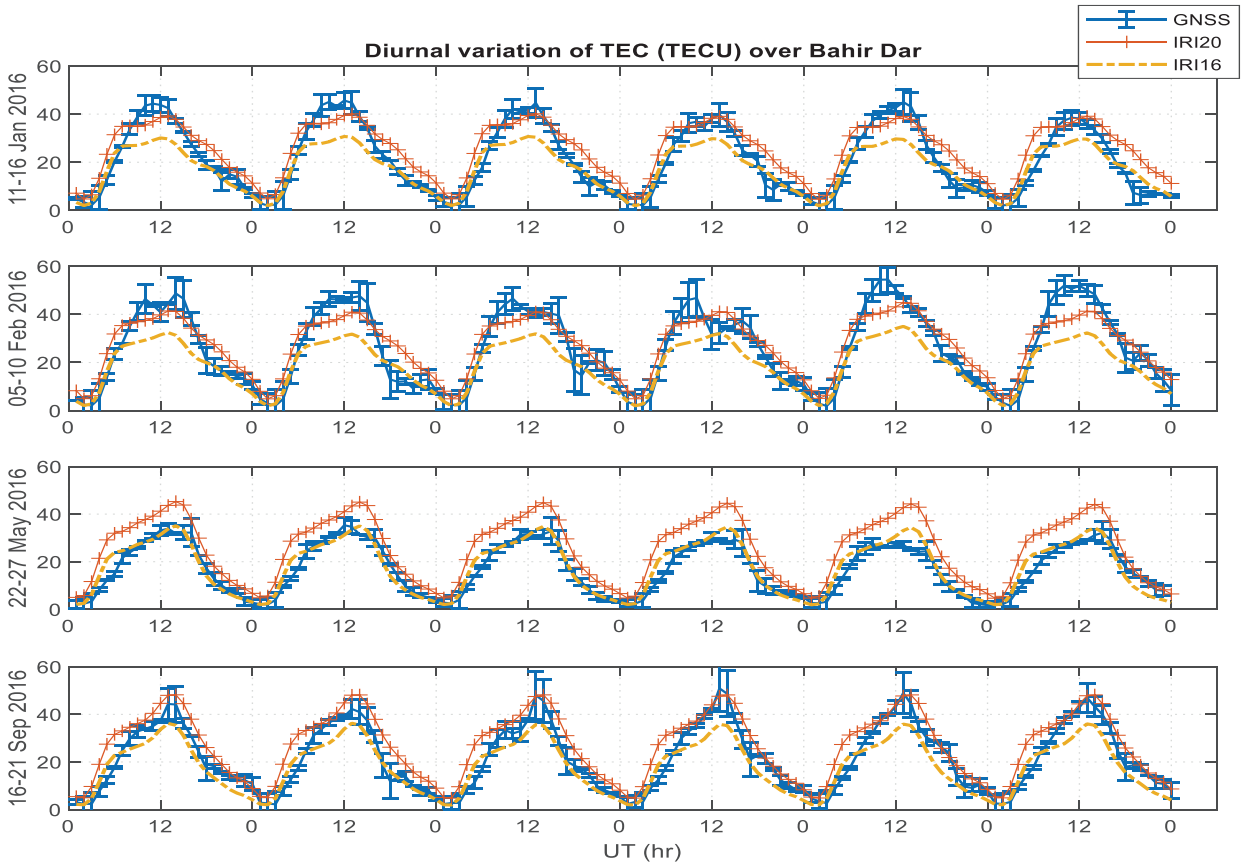

Fig. 6. Similar to Fig. 1, but for Bahir Dar station.

ward) does not exceed 60 TECU, whereas on the third panel, all the recorded measurements during all phases of the storm are greater than 60 TECU. Thus, IRI-2020 and IRI-2016 show the best performances, especially during storms and seasons with enhanced TEC over Sheba. However, in most cases (hours of a day, season, or month), the IRI-2016 estimates are slightly smaller than the IRI-2020 predictions. A more general evaluation of the IRI models can be drawn after a look at the performances at some more stations described below.

3.2. Performance of IRI over Bahir Dar

In Fig. 6, we presented a similar analysis to Fig. 1 for the Bahir Dar GPS station. From the first panel (count downward), we noticed that both model versions agreed with the observed TEC from 00:00 to about 06:00 UT. From about 07:00 to 15:00 UT, IRI-2020 slightly underestimated; however, IRI-2016 shows even larger differences than IRI-2020 compared to the observed TEC. Exceptionally, on the 14th and 16th of January 2016 (look at the 4th and 6th days counting from left), both models showed a good fit to the observed TEC. On the second panel, the observed TEC peaks are much greater, and under-estimations increased in magnitude over the peak hours. A similar comparison is presented on the third and fourth panels, and we will have generalizations in the conclusion section.

From Fig. 7, it is shown that the IRI-2020 model well agreed with the GPS observations on the March equinox from 08:00 UT to 16:00 UT, but discrepancies of about 10 TECU are also seen at about 18:00 UT and an hour before and after. At the September equinox and June solstice, IRI-2020 overestimated the observed TEC at almost all times of the day except from 01:00 to 04:00 UT. IRI-2016 fitted well with the observed TEC during the night (01:00 to 05:00 UT and 21:00 to 24:00 UT) as compared to the estimations by IRI-2020. From these seasonally averaged plots of TEC, it is also possible to notice that the times of peaks are well predicted by both IRI model versions. Seasonal analysis shows that IRI-2016 shows an excellent fit to the GPS observations during the whole day except between 09:00 and 15:00 UT in the case of the September equinox and the December solstice. But larger underestimations are seen during daytime hours at the March equinox. We noticed excellent predictions by the IRI-2016 for the June solstice. Though discrepancies are evident from the seasonal analysis or plots, both models are in a good position to inform society about the state of the ionospheric density over Bahir Dar station. However, we suggest future modifications to the IRI-2020 TEC profile to consider adding more data from this region.

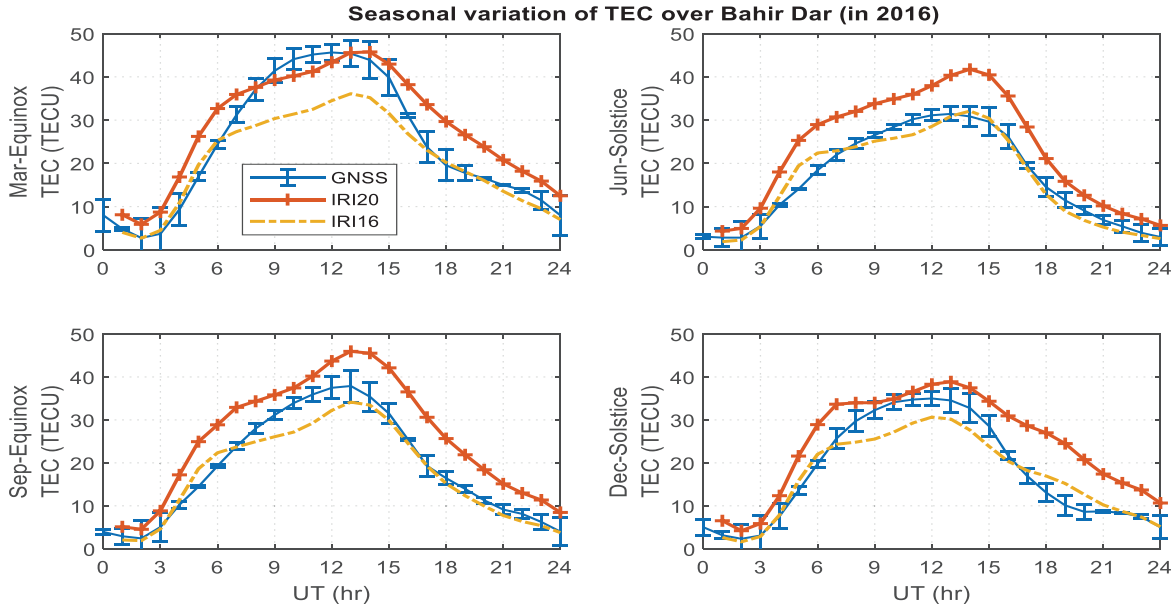

Fig. 7. Similar to Fig. 2, but for Bahir Dar station.

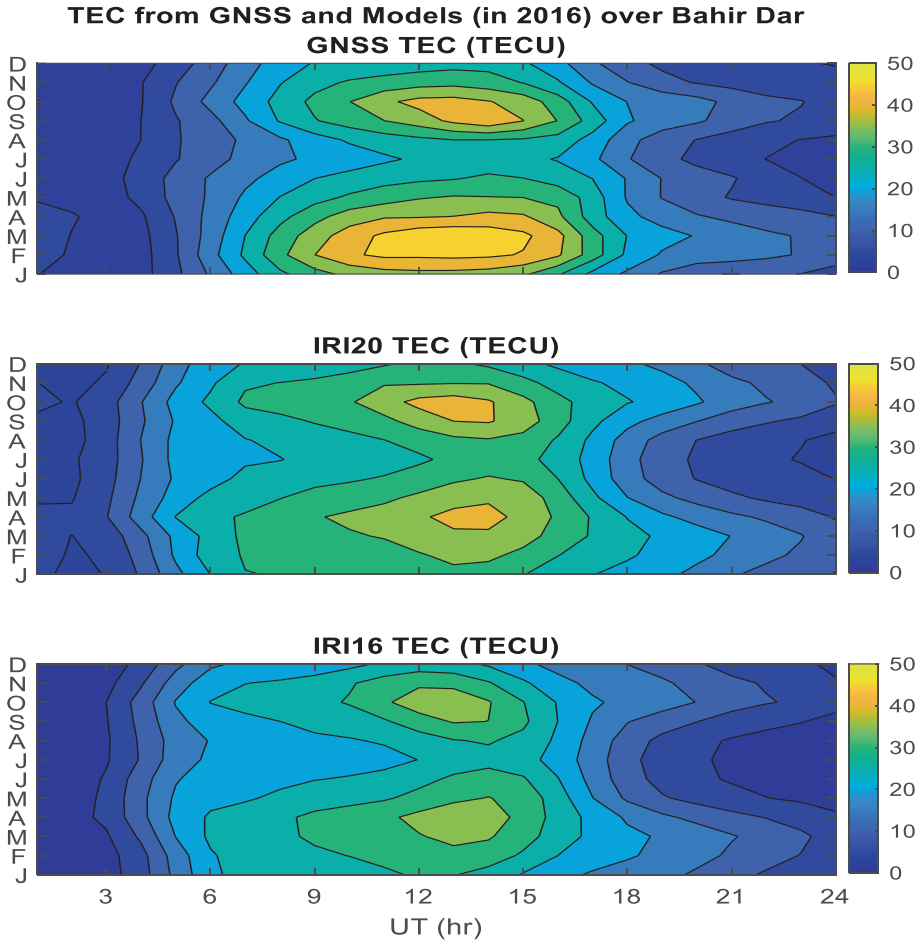

Fig. 8. Similar to Fig. 3, but for Bahir Dar station.

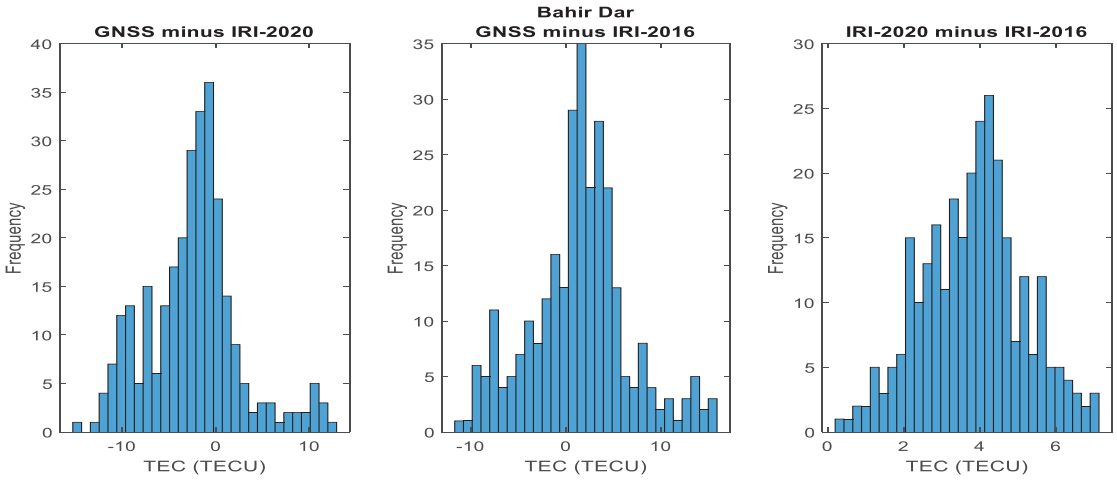

Fig. 9. Similar to Fig. 4, but for Bahir Dar station.

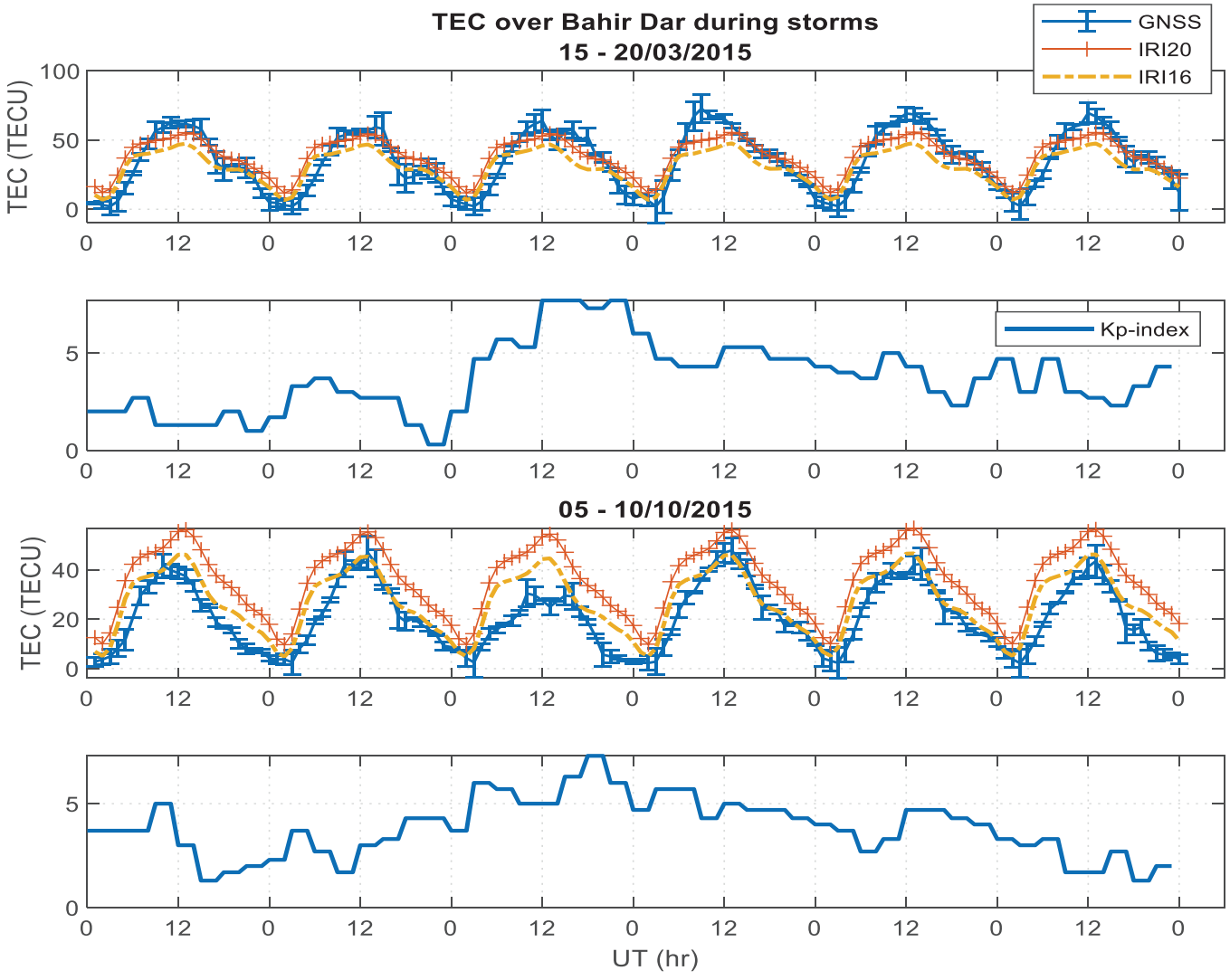

Fig. 10. Similar to Fig. 5, but for Bahir Dar station.

This is because the most probable cause of mismodeling in the African sector is believed to be a scarcity of observations.

In Fig. 8, the mean monthly vertical TEC profile over Bahir Dar station is presented using GPS, IRI-2020, and IRI-2016. If a reader notes each similar color from the models and the GPS contour plots, the differences between the predicted (model) values and the measured values will be clearly seen there. Moreover, the histograms in Fig. 9 show more quantitative and statistical evaluations of the model predictions. These histogram analyses in Fig. 9 clarify how efficient the estimations of the models are for the observed TEC. The first panel (from left) indicates a higher frequency of values (data points) between ± 5 TECU. This panel shows the difference between the observed and IRI-2020 predicted TEC over Bahir Dar. However, a few of the observed TECs are poorly estimated (i.e., differences up to ± 15 TECU). Negative differences result from the IRI-2020 overestimations. The reader can see a similar comparison picture in the middle panel of Fig. 9 for observed TEC and IRI-2016 TEC. The third panel (from left) shows the gaps between IRI-2020 and IRI-2016 estimates.

Over Bahir Dar, storm time validations are presented in Fig. 10. The storm on March 17, 2015, shows a higher Kp index value of ∼ 8.0 (i.e., see the second panel (count downward)). It caused a positive ionospheric storm that enhanced TEC (i.e., from quiet time averages in March/2015). Both IRI-2020 and IRI-2016 show excellent agreement with the observed TEC in other hours of the day (except peak TEC hours) during all the initial, main, and recovery phases of the storm. Both models underestimated the peaks, predicting 10 to 15 TECU lower than the observed TEC.

A storm event on October 7, 2015, with Kp ∼ 7.0, affects the ionospheric TEC negatively (see the third and fourth panels of Fig. 10, (count downward)). Especially during the main phase, the smallest GPS-TEC is recorded compared to the initial and recovery phases of the storm. The observed TEC agreed with IRI-2016 estimates except for the main phase of the storm. During the main phase, GPS recorded a peak value that was not greater than 33 TECU; the peak of IRI-2020 was greater than 55 TECU; and the peak of IRI-2016 was about 50 TECU.

3.3. Performance of IRI over Turkwel

The third station considered in our work is Turkwel, Kenya. Fig. 11 shows the diurnal variation of quiet time TEC from GPS, IRI-2020, and IRI-2016. Like what we

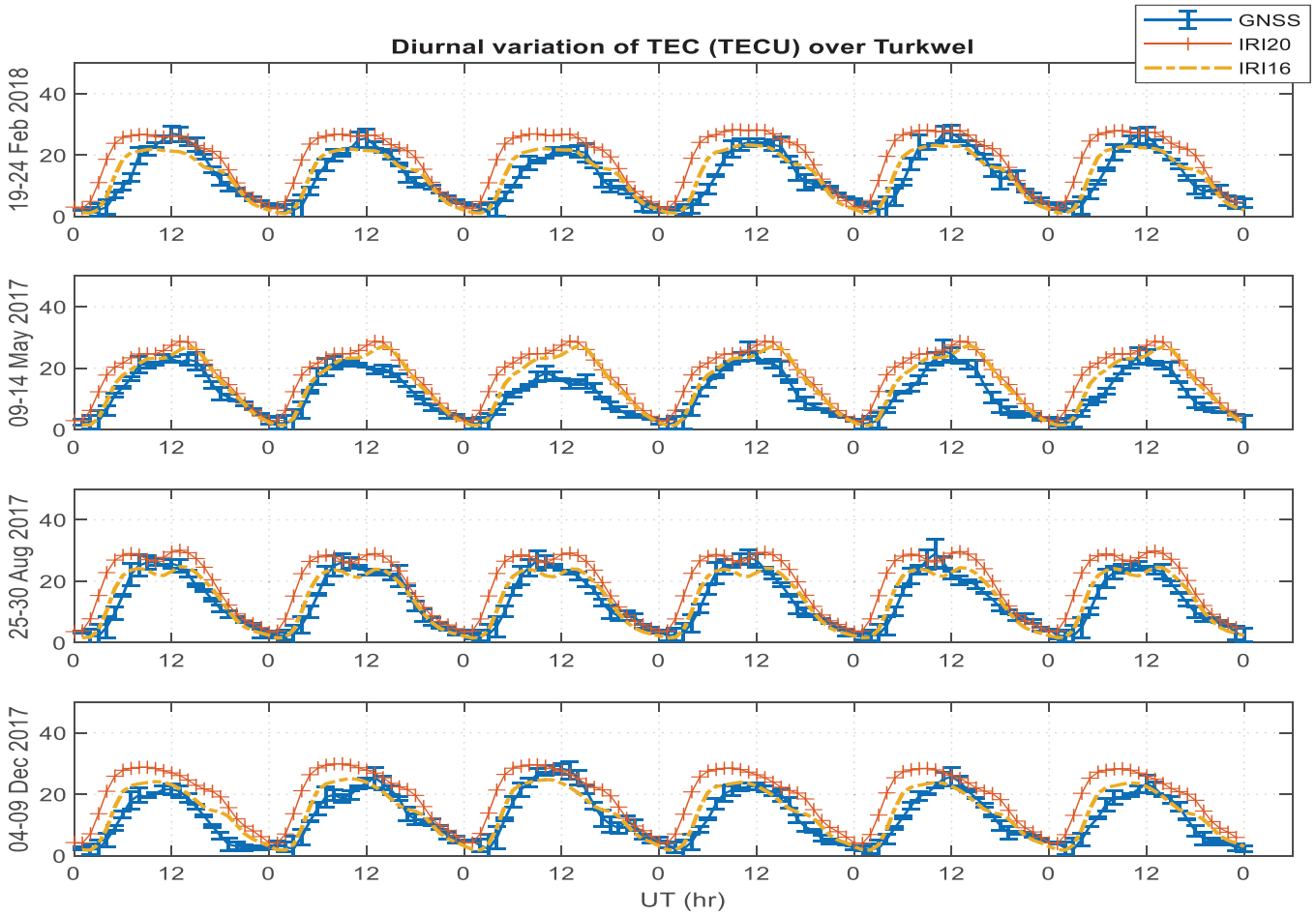

Fig. 11. Similar to Fig. 1, but for Turkwel station.

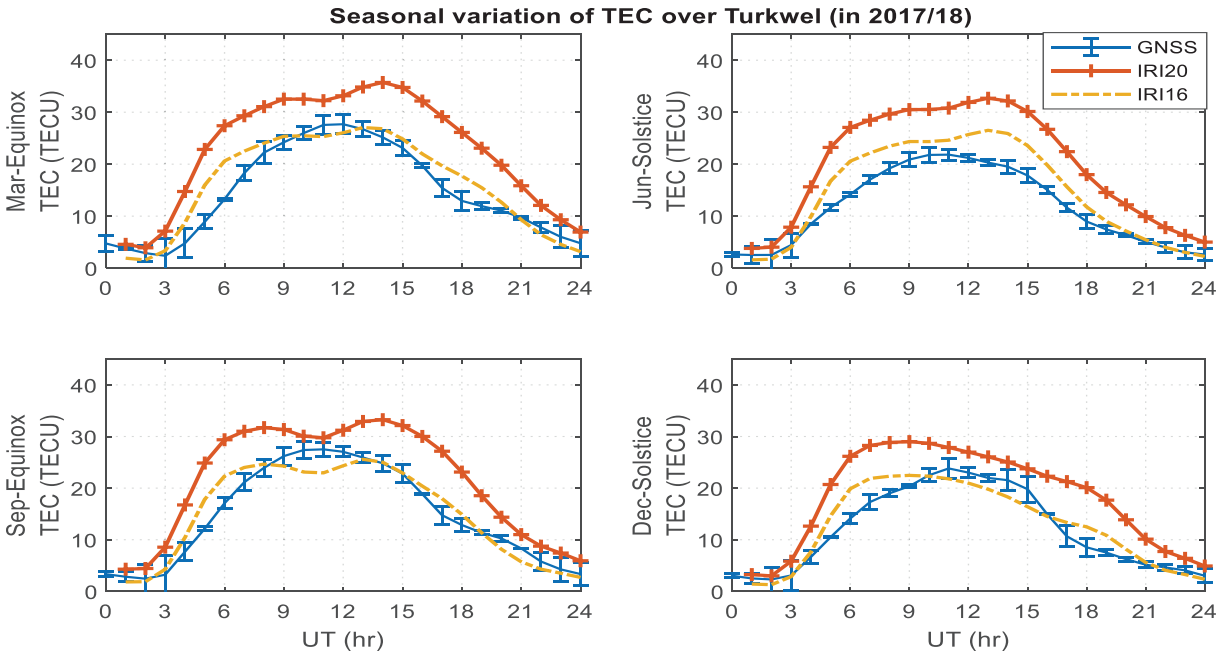

Fig. 12. Similar to Fig. 2, but for Turkwel station.

did to the above stations (Sheba and Bahir Dar), six consecutive days roughly representing each of the four seasons are presented. The top panel (19–24 February 2018) depicts an overstimulation of the observed TEC by IRI-2020 in almost all hours of the day. An excellent fit to the observed TEC is seen by the IRI-2016 during all six consecutive days. The IRI-2020 predicted TEC gets its peak value an hour earlier than the GPS observations. The second panel (for May 9–14, 2017) shows predictions by IRI-2020 overestimating in all days and hours, but with smaller differences (not greater than 5 TECU on average). GPS receivers recorded smaller TEC values in all the panels of Fig. 11. The average TEC recorded is 20 TECU, and the maximum is about 25 TECU. Generally, the diurnal analysis of the model validation shows excellent fits between IRI-2016 and observed TEC on almost all days. The double peak estimates by both models from August 25–30, 2017 are not observed on the observed TEC.

Fig. 12 represents the seasonal variation of TEC with models and observations. The plots indicate noticeable overestimations by the IRI-2020 model and relatively good performance by the IRI-2016 version. In the September equinox, both model versions show two nearly equal peaks at about 8:00 UT and 14:00 UT (see also diurnal patterns in Fig. 11; 25–30/08/2017); however, the observation does not confirm this scenario. This implies that the models need further regional improvements to capture and predict these low TEC profiles. In Fig. 13, the reader can easily compare and contrast the corresponding time colors of the contours of GPS-TEC, IRI-2020, and IRI-2016 TECs to examine the power of the models in estimating the observed TEC. Moreover, the differences between models and measurements are presented in Fig. 14 for statistical evaluation. For instance, from the first panel on Fig. 14, the difference between GPS-TEC and IRI-2020 TEC shows overestimations up to 15 TECU and under-estimations up to 5 TECU. However, much of the difference lies in the range of −10 TECU and 2 TECU and is evident from the good predictions by IRI-2020. But IRI-2016 shows better predictions than IRI-2020 because much of the difference lies in the range of −5 TECU to 5 TECU.

Fig. 15 represents geomagnetic storm effects on GPS-TEC and TEC derived from the IRI-2020 and IRI-2016 models. Similar to the storm time validations above, two storm events and six consecutive days for each event are considered to assess the performance of the models. During a storm on September 8, 2017, the peaks of the observed TEC and IRI-2020 agreed. The double peak predictions of IRI-2020 agreed to some extent on the initial and main phases of the storm, but discrepancies were up to 20 TECU on the last recovery day in our analysis (on September 11, 2017). IRI-2016 significantly underestimated the peak values. During a storm on August 26, 2018, IRI-2020 overestimated the observed TEC. Comparing the magnitude, the observed TEC during the 06–11/09/2017 storm is greater than the TEC recorded from 24 to 29/08/2018. IRI-2016 best performs when observed TEC values get lower, while IRI-2020 performs well when the measurements are significantly greater than the quiet time average TEC (i.e., in the same season).

3.4. Performance of IRI over Arequipa

The daily variation of TEC over Arequipa, Peru, and the validations of the IRI models are presented in Figs. 16–20. In Fig. 16, the top panel is for days 03–08/04/2021; the second panel (from the top) is for days 22–27/06/2021; the third panel is for days 08–13/09/2021, and the last-bottom

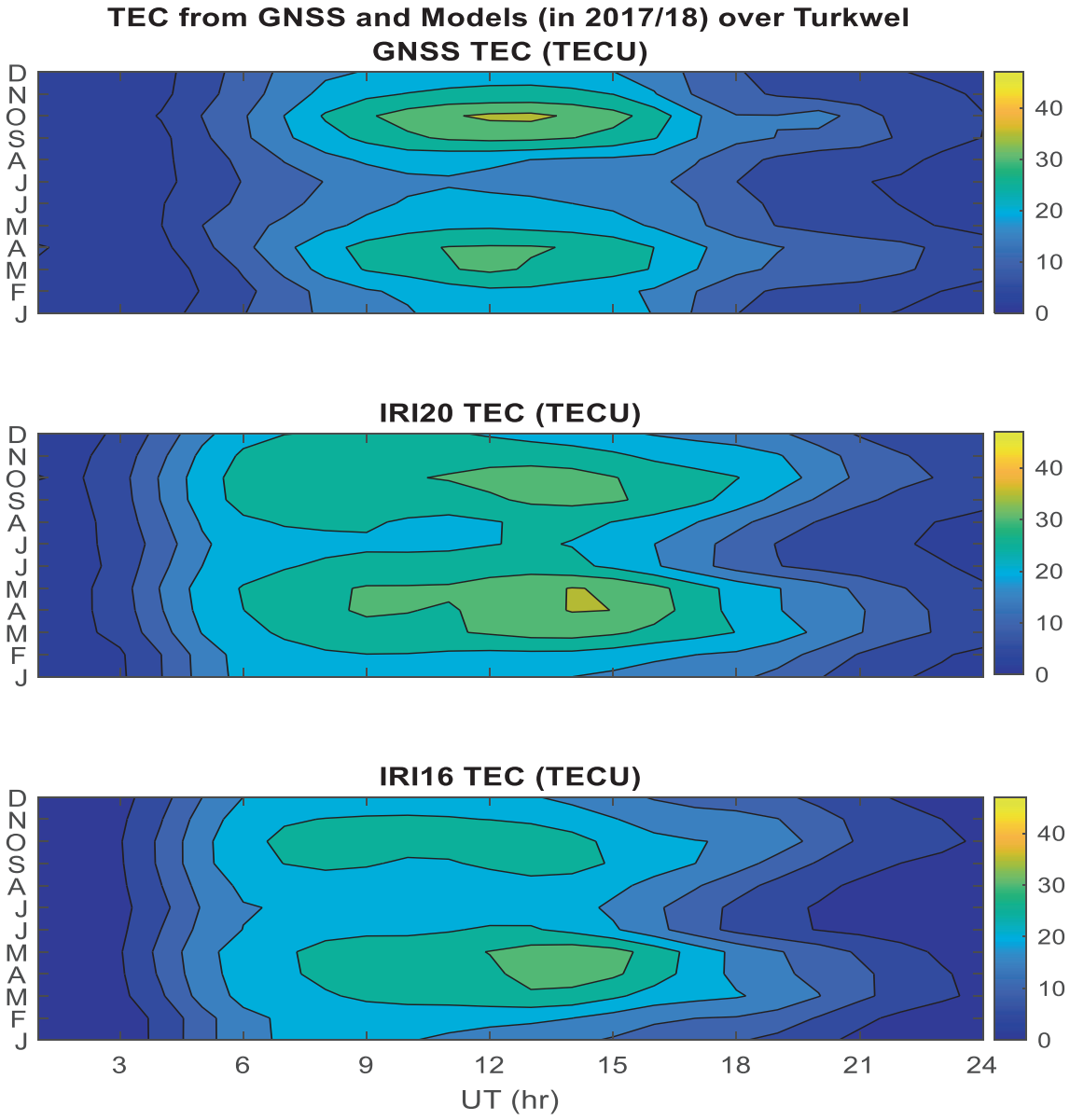

Fig. 13. Similar to Fig. 3, but for Turkwel station.

panel is for days 16–21/12/2021. On the top panel, double peaks estimated by IRI-2016 and IRI-2020 are not reflected by the observed TEC. The discrepancies are high on all days except from 09:00 to 12:00 UT. On the same panel, IRI-2016 shows much better performance than IRI-2020. The peak hours are similar to all models as well as the observed TEC. On the second panel, IRI-2016 shows the best fit to the observed TEC, and IRI-2020 performs better compared to the days in the first panel. Both models and the observed values show troughs at nearly the same time. In general, except as shown on the first panel, the diurnal variation over Arequipa shows excellent fits between the observed and model values.

The curves in Fig. 17 are to compare the seasonal averaged predictions of the IRI models with the GPS-measured TEC. The top panel on the left (for the March equinox) shows an excellent fit between the observed TEC and IRI-2016 estimates at all hours of the day. IRI-2020 agrees with measured values from about 08:00 to 11:00 UT and from about 16:00 to 18:00 UT. The seasonal averaged curves exhibit greater in-phase trends (troughs and peaks of observed and model TECs occur concurrently). Both model versions show overestimation during the whole day of the September equinox. Similar characteristics are reflected in all seasons over Arequipa. But the averaged seasonal IRI-2016 TEC agreed with the observed values during almost all hours of the day at the March equinox and December solstice. In Fig. 18, like the analysis we presented to the other stations, monthly averaged TEC contour plots are done. Histogram on the left side of Fig. 19 shows that IRI-2020 over-estimated almost all the observed TEC (i.e., over 50% of a $12 \times 24 = 288$ monthly averaged

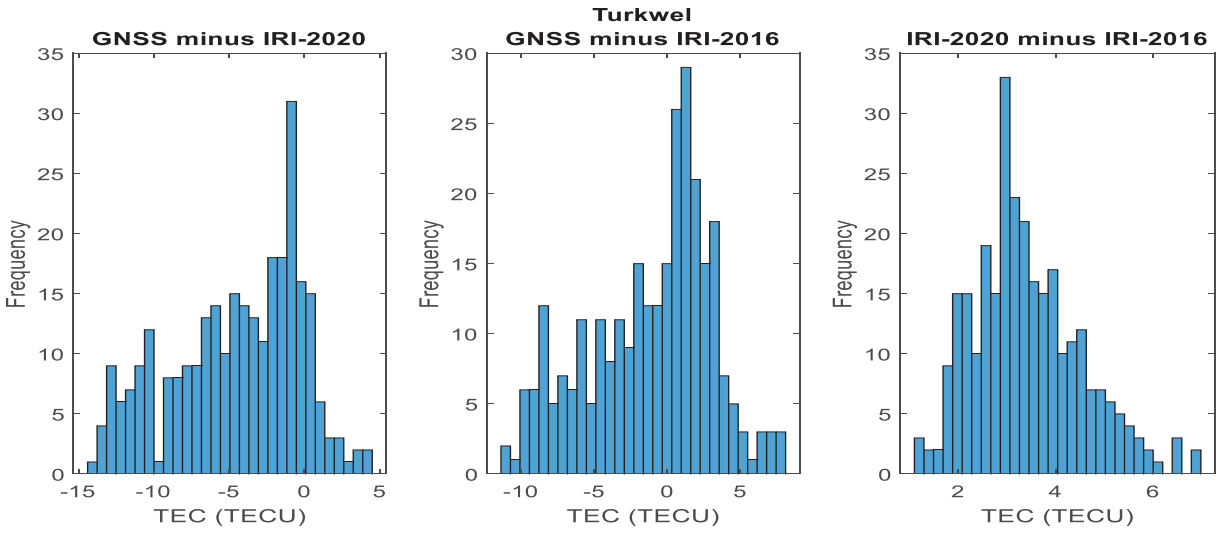

Fig. 14. Similar to Fig. 4, but for Turkwel station.

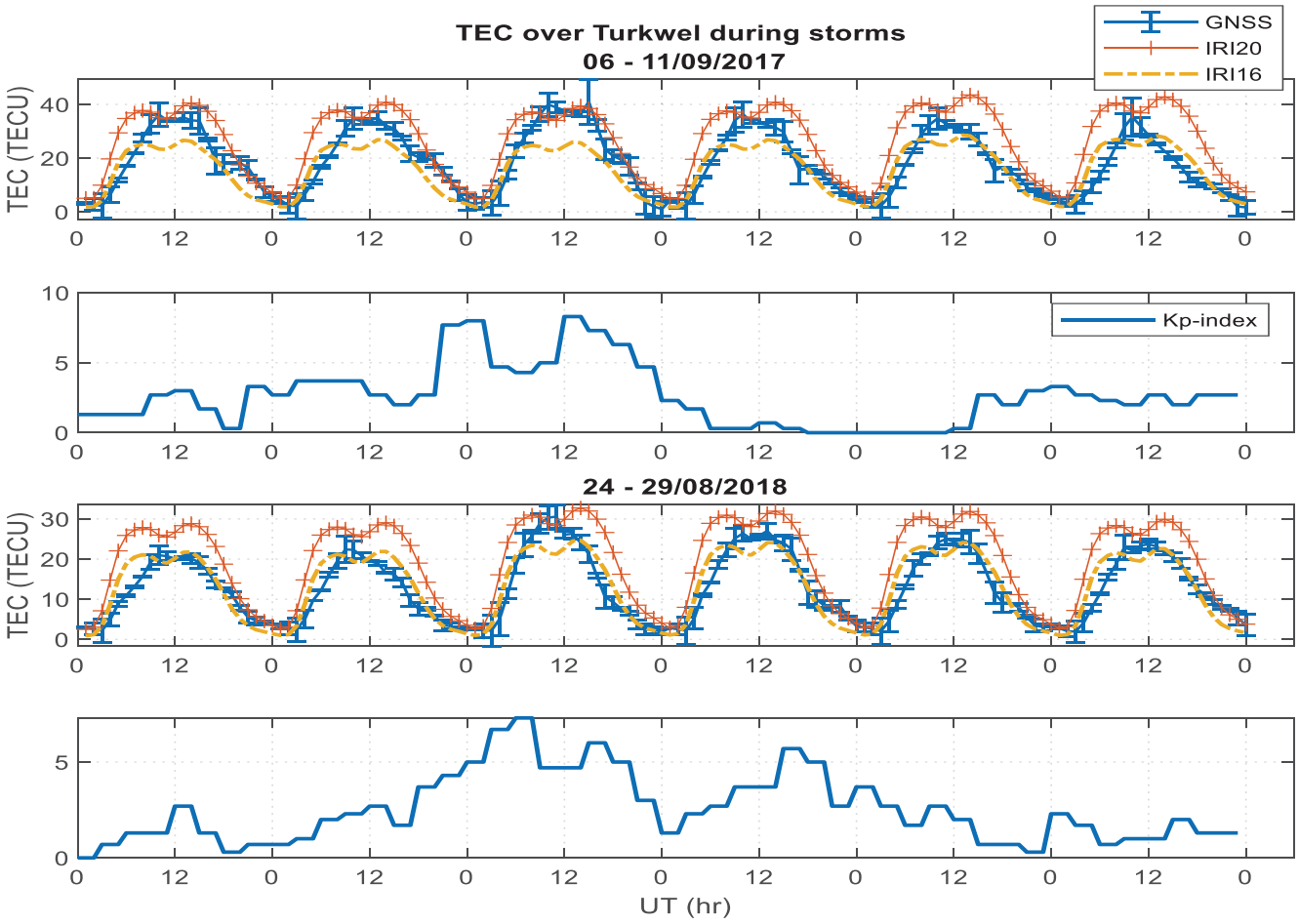

Fig. 15. Similar to Fig. 5, but for Turkwel station.

observed TEC is over-estimated with differences ranging from 5 to 18 TECU (magnitude)). Relative to IRI-2020, the IRI-2016 predictions show very good agreement with the observed TEC. That is, over 90% of the $12 \times 24 = 2$ 88 averaged observed TEC data is either under- or over-estimated, with differences only up to 5 TECU (magnitude). A storm-time diurnal analysis result is presented in Fig. 20. Both models underestimated the peak of the storm

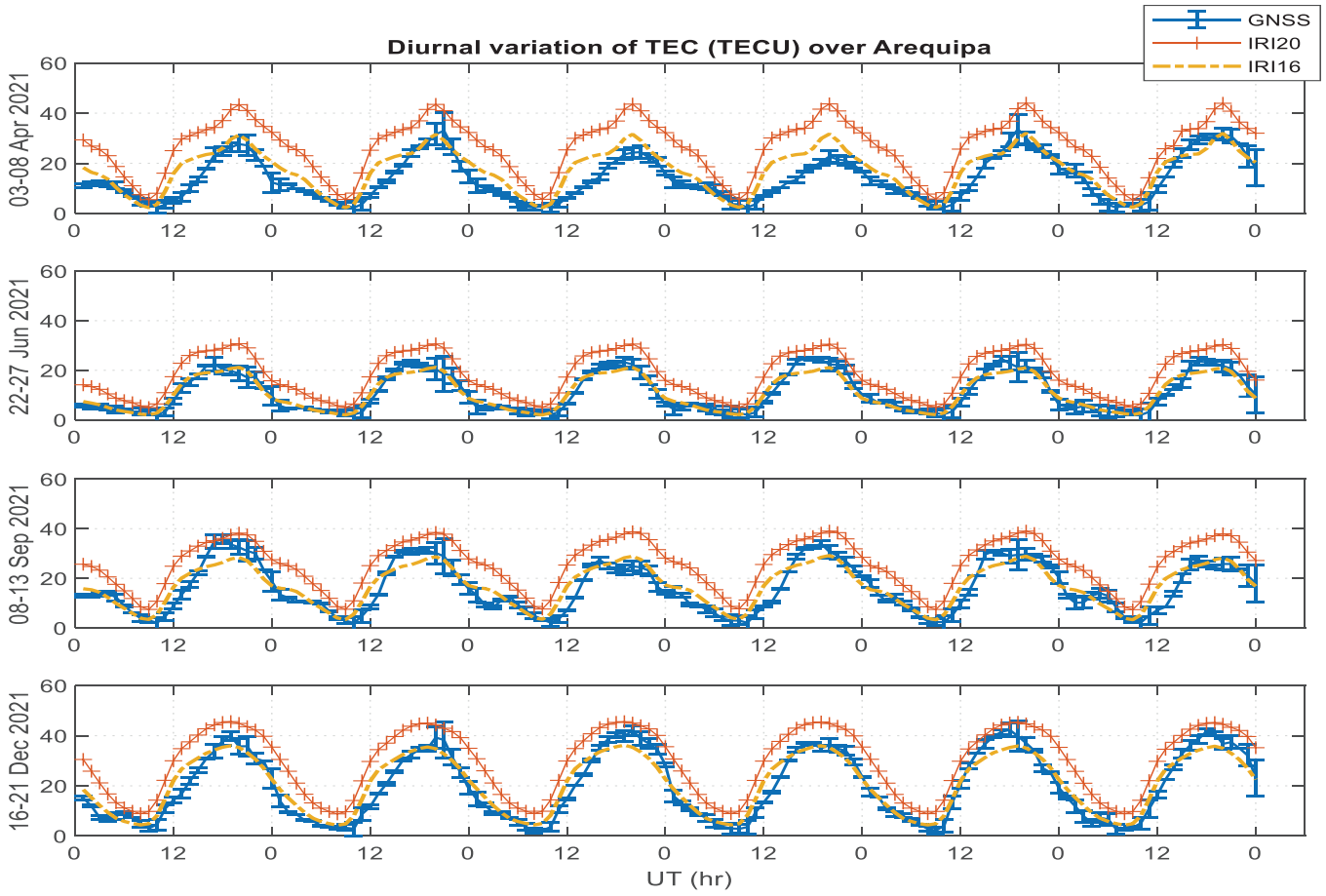

Fig. 16. Similar to Fig. 1, but for Arequipa station.

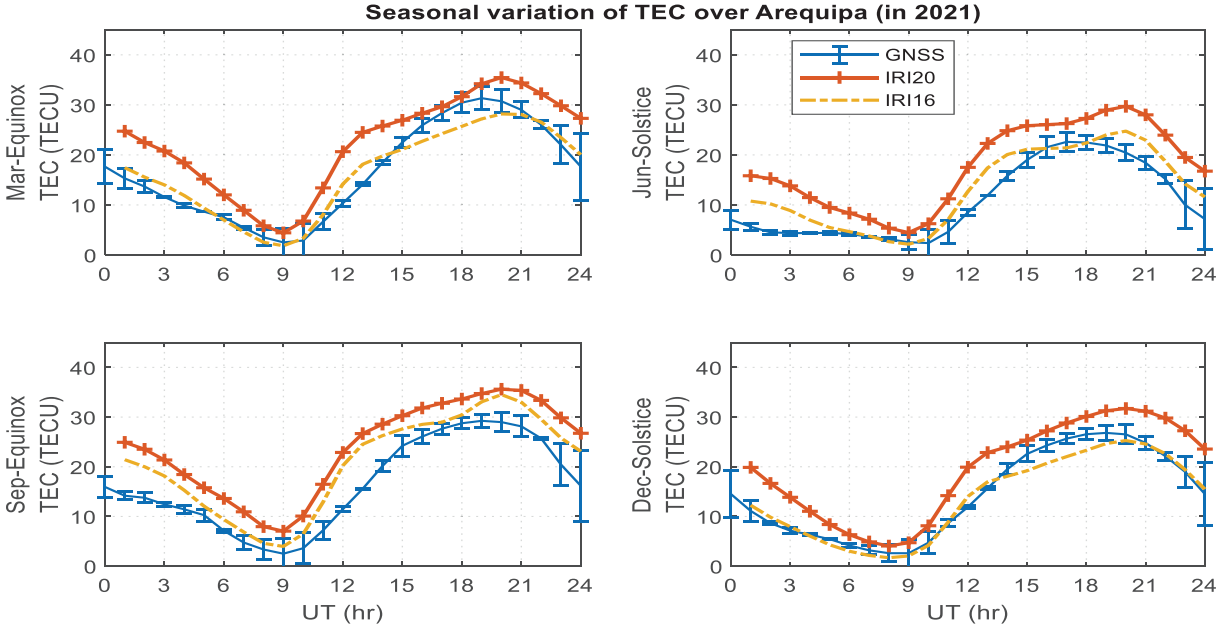

Fig. 17. Similar to Fig. 2, but for Arequipa station.

day observed TEC (08/09/2017, which is a day of the main storm phase). IRI-2016 underestimated, with larger discrepancies from about 17:00 to 21:00 UT. The models agreed with the observed TEC in the initial and recovery phases of the storm. The observed TEC showed much smaller amplitude during the August 26, 2018 storm. IRI

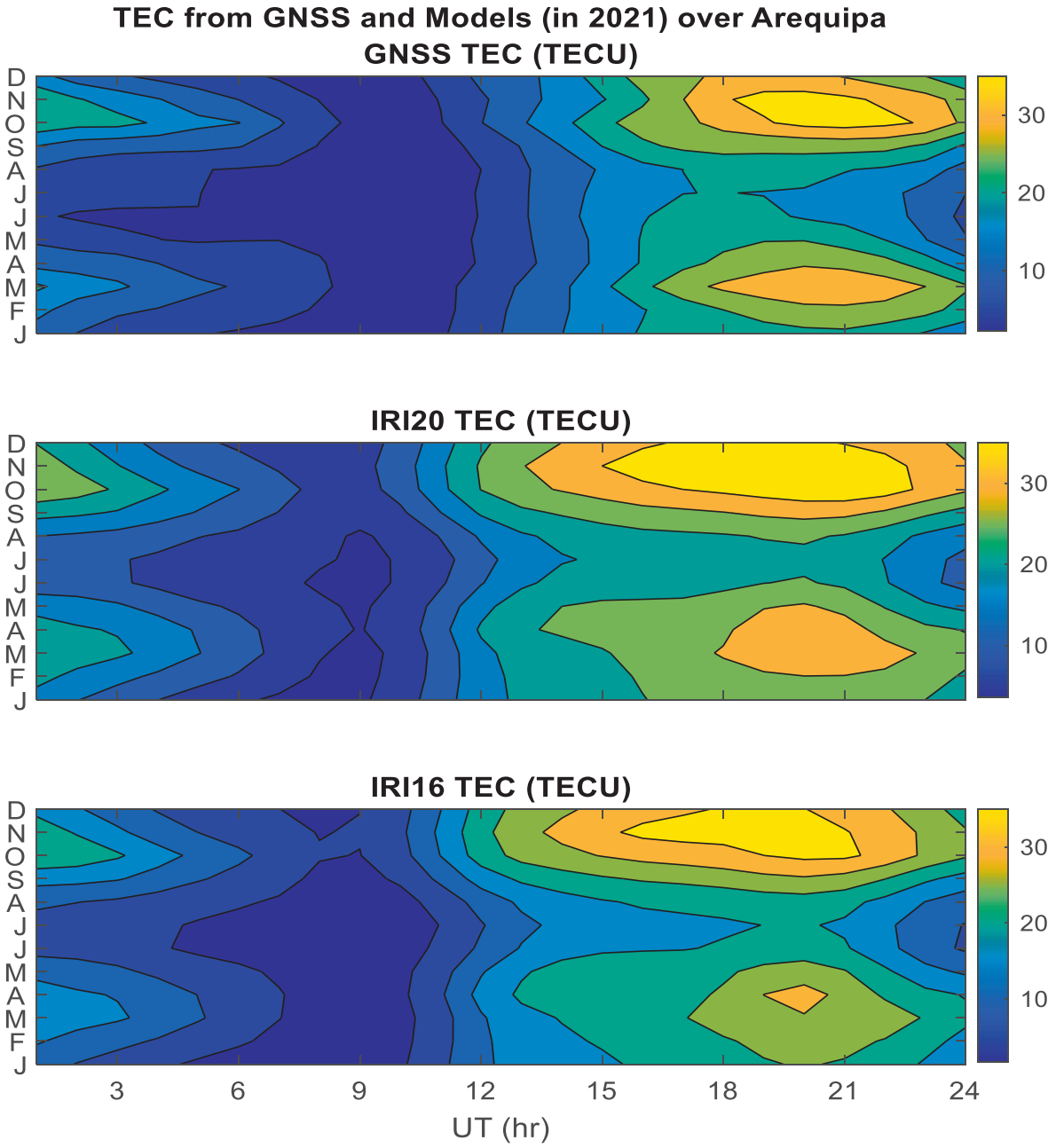

Fig. 18. Similar to Fig. 3, but for Arequipa station.

models show good agreement with the observed TEC in all phases of this storm.

4. Dicussion and conclusions

This study evaluated the performance of the IRI (IRI-2016 and IRI-2020) ionospheric data-driven empirical model in describing both quiet-time and disturbed-time characteristics of the equatorial region ionosphere using GPS stations in east Africa and south America. This is carried out by comparing the vertical TEC from ground GPS receivers with corresponding values computed using the model. Different and possible types of approaches are applied to present effective validation work. Diurnal, seasonal, monthly, and storm time analyses have been performed for each station. Six consecutive quiet days are selected from each season of a year to evaluate the diurnal performance of IRI-2016 and IRI-2020. All available quiet-day GPS-TECs of each season are averaged to have a single mean TEC curve. Similarly, we did this for TEC from IRI-2016 and IRI-2020 and compared the model estimates with the observed TEC. Likewise, monthly averaged observed TEC and model estimates are compared. Histograms for statistical quantification are also presented, and lastly, we plotted storm time diurnal TEC and compared the observed TEC over each station with the model estimates. Two geomagnetic storm days for each station are selected, and the analysis covers the initial, main, and

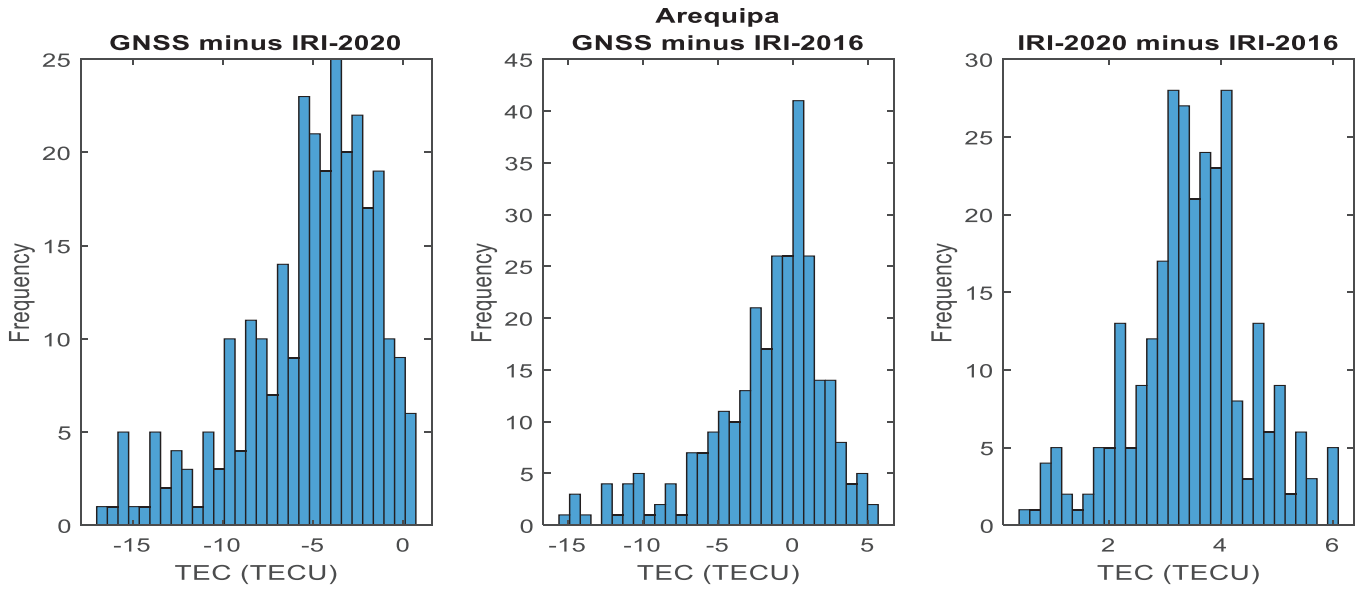

Fig. 19. Similar to Fig. 4, but for Arequipa station.

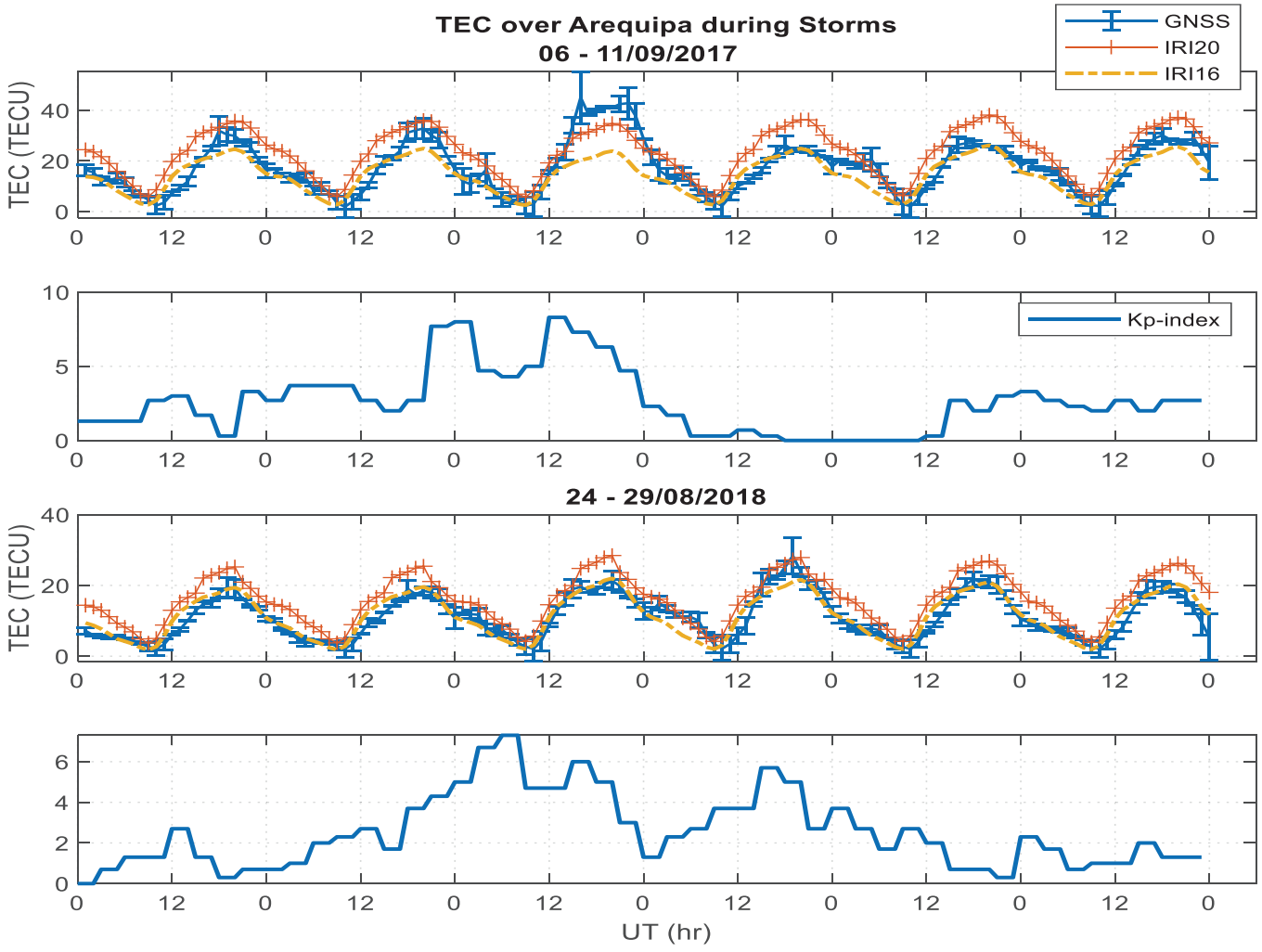

Fig. 20. Similar to Fig. 5, but for Arequipa station.

recovery phases. The study screened out instances of best estimations and mismodeling for further improvements.

Validations are done using the 2012 and 2013 experimental TEC over Sheba and the 2015 and 2016 observed TEC over Bahir Dar station. These years are in the period of the solar cycle maximum (solar cycle 24). The TEC observations used for Turkwel are from 2017 and 2018, and for Arequipa from 2021. Years 2017, 2018, and 2021 are in the period of the solar cycle minimum (i.e., a trough between solar cycles 24 and 25). Thus, we found it important to discuss the results considering the solar conditions as well. Generally, discrepancies noted between the models' and the observed TEC tend to decrease when the observed TEC attains a greater magnitude compared to the quiet time average. In addition, we found IRI (both versions) showing better agreement with the observed TEC during the solar cycle maximum periods. Comparing the curves in Figs. 1 and 6 with Figs. 11 and 16, it is easy to visualize that the observed TEC shows high magnitudes during the solar maximum. As far as this result is concerned, IRI best reproduced/forecasted enhanced TEC measurements.

The seasonal evaluation over Turkwel shows that IRI-2020 produces double peak profiles on the March equinox, June solstice, and September equinox and is overestimated with larger discrepancies. Over the other three stations, both IRI versions reproduced the seasonal averaged observed TEC (both the amplitude and the phase) with only slight gaps/differences. We also quantified the discrepancies using histograms, which enabled us to calculate the percentage of larger mismodeling.

In most cases, the values of the IRI-2020 model exceed the observational values. When we think of plasmaspheric effects on our comparisons, Yzengaw et al. (2008) reported that the plasmaspheric contribution exhibits a diurnal variation that depends on latitude. They also presented a percentage contribution indicating minimum contribution of 10% (sun-side) and a maximum contribution of 60% (nigh-side). The contribution is high in the equatorial region because of the long distance the GPS ray travels through the plasmasphere. Besides, we should mention that the solar cycle variation of the plasmaspheric contribution has its own effect on the measured TEC as well. It is mentioned in Bilitza et al. (2022) that, optionally, one can extrapolate the topside density and temperature formulas to plasmaspheric heights to include the plasmasphere contributions. Thus, if the contributions from the plasmasphere are added to the TEC from the IRI model, as most of the cases indicate, IRI-2016 fits the observed TEC with slight overestimations and agrees with the results reported and reviewed in the introduction section. But the gaps between IRI-2020 and observed TEC increase when this plasmaspheric effect adds to the model.

Generally, the following concluding points can be drawn out of this study:

- IRI-2020 overestimates the observed TEC in almost all cases except on some occasions over Bahir Dar station.
- Both IRI versions show better predictions over Arequipa, Peru, than other stations in east Africa.
- Even though all IRI versions are poor at predicting storm effects over low latitudes, in our work, probably by chance, during storms, IRI-2020 better inferred positively enhanced GPS-TEC than IRI-2016.
- Exceptionally, during the storm on March 17, 2015, IRI-2020 under-estimated the storm-enhanced TEC over Bahir Dar station at all phases of the storm.
- However, both model versions do not show the storm effects observed on GPS-TEC.
- Including latest observations from the African and south American regions will definately enable IRI-2020 model to perform even better.

5. Availability of data and materials

The authors would like to thank the community of UNAVCO (https://www.unavco.org/) for the GPS-TEC data. Kp index data are provided by the National Aeronautics and Space Administration's (NASA's) Space Physics Data Facility via https://omniweb.gsfc.nasa.gov/. The British Geological Survey (BGS) web-based tools via https://www.geomag.bgs.ac.uk are used for conversion from geographic to geomagnetic coordinates. IRI-2020 and IRI-2016 are downloaded from the Community Coordinated Models Center of NASA via https://kauai.ccmc.gsfc.nasa.gov/instantrun/iri. A Figshare profile for the corresponding author is at https://figshare.com/authors/Habtamu_Alemu/15186637.

Funding

The first author is partially supported by a project from the Institute of Atmospheric Physics, Czech Academy of Sciences, Czechia, under grant number 560823AHA.

Declaration of Competing Interest

The authors declare that they have no known competing financial interests or personal relationships that could have appeared to influence the work reported in this paper.

Acknowledgments

We would like to thank Institute of Atmospheric Physics of the Czech Academy of Sciences, Czechia, for the funding support. The authors are also very grateful to UNAVCO (for vertical TEC data) and NASA (for OMNIweb calculated Kp-index and IRI-2020 and IRI-2016 instant run access) and the British Geological Survey (BGS) for providing coordinate conversion web-based tools. We also thank Dr. Gopi K. Seemala of the Indian Institute of Geomagnetism for his free access GPS-TEC analysis softwere.

References

Arikan, F., Sezen, U., Gulyaeva, T.L., 2019. Comparison of IRI-2016 F2 layer model parameters with ionosonde measurements. J. Geophys. Res. 124 (10), 8092–8109. https://doi.org/10.1029/2019JA027048.

Bilitza, D., Pezzopane, M., Truhlik, V., Altadill, D., Reinisch, B. W., & Pignalberi, A. (2022). The International Reference Ionosphere model: A review and description of an ionospheric benchmark. *Reviews of Geophysics*, *60*(4), e2022RG000792.

Bilitza, D., Xiong, C., 2021. A solar activity correction term for the IRI topside electron density model. Adv. Space Res. 68 (5), 2124–2137. https://doi.org/10.1016/j.asr.2020.11.012.

Chen, J., Ren, X., Zhang, X., Zhang, J., & Huang, L. (2020). Assessment and validation of three ionospheric models (IRI-2016, NeQuick2, and IGS-GIM) from 2002 to 2018. *Space Weather*, *18*, e2019SW002422. https://doi.org/ 10.1029/2019SW002422.

Endeshaw, L., 2020. Testing and validating IRI-2016 model over Ethiopian ionosphere. Astrophys. Space Sci. 365 (3), 49.

Ezquer, R.G., López, J.L., Scidá, L.A., Cabrera, M.A., Zolesi, B., Bianchi, C., Mosert, M., 2014. Behaviour of ionospheric magnitudes of F2 region over Tucumán during a deep solar minimum and comparison with the IRI 2012 model predictions. J. Atmos. Sol. Terr. Phys. 107, 89–98.

Fejer, B.G., Jensen, J.W., Su, S.Y., 2008. Quiet time equatorial F region vertical plasma drift model derived from ROCSAT-1 observations. J. Geophys. Res. Space Phys. 113 (A5).

Friedrich, M., Pock, C., Torkar, K., 2018. FIRI-2018, an updated empirical model of the lower ionosphere. J. Geophys. Res. Space Phys. 123 (8), 6737–6751. https://doi.org/10.1029/2018JA025437.

Galkin, I., Froń, A., Reinisch, B., Hernández-Pajares, M., Krankowski, A., Nava, B., Batista, I., 2022. Global monitoring of ionospheric weather by GIRO and GNSS data fusion. Atmos. 13 (3), 371.

Kauristie, K., Andries, J., Beck, P., Berdermann, J., Berghmans, D., Cesaroni, C., Österberg, K., 2021. Space weather services for civil aviation—challenges and solutions. Remote Sens. (Basel) 13 (18), 3685.

Marew, H., Nigussie, M., Hui, D., Damitie, B., 2019. A method of estimating equatorial plasma vertical drift velocity and its evaluation using C/NOFS observations. Radio Sci. 54 (7), 590–601.

Moses, M., Bilitza, D., Panda, S.K., Ochonugor, B.J., 2021. Assessment of IRI-2016 hmF2 model predictions with COSMIC observations over the African region. Adv. Space Res. 68 (5), 2115–2123.

Nigussie, M., Radicella, S.M., Damtie, B., Nava, B., Yizengaw, E., Groves, K., 2013. Validation of the NeQuick 2 and IRI-2007 models in East-African equatorial region. J. Atmos. Sol. Terr. Phys. 102, 26–33.

Nigussie, M., Radicella, S.M., Damtie, B., Yizengaw, E., Nava, B., Roininen, L., 2016. Validation of NeQuick TEC data ingestion technique against C/NOFS and EISCAT electron density measurements. Radio Sci. 51 (7), 905–917.

Ogwala, A., Somoye, E.O., Panda, S.K., Ogunmodimu, O., Onori, E., Sharma, S.K., Oyedokun, O., 2021. Total electron content at equatorial and low-, middle-and high-latitudes in African longitude sector and its comparison with IRI-2016 and IRI-PLAS 2017 models. Adv. Space Res. 68 (5), 2160–2176.

Ogwala, A., Oyedokun, O.J., Ogunmodimu, O., Akala, A.O., Ali, M.A., Jamjareegulgarn, P., Panda, S.K., 2022. Longitudinal Variations in Equatorial Ionospheric TEC from GPS, Global Ionosphere Map and International Reference Ionosphere-2016 during the Descending and Minimum Phases of Solar Cycle 24. Universe 8 (11), 575.

Pignalberi, A., Pietrella, M., Pezzopane, M., 2021. Towards a real-time description of the ionosphere: A comparison between International Reference Ionosphere (IRI) and IRI real-time assimilative mapping (IRTAM) models. Atmos. 12 (8), 1003. https://doi.org/10.3390/atmos12081003.

Scidá, L.A., Ezquer, R.G., Cabrera, M.A., Mosert, M., Brunini, C., Buresova, D., 2012. On the IRI 2007 performance as a TEC predictor for the South American sector. J. Atmos. Sol. Terr. Phys. 81, 50–58.

Tariku, Y.A., 2015. TEC prediction performance of IRI-2012 model during a very low and a high solar activity phase over equatorial regions, Uganda. J. Geophys. Res. Space Phys. 120 (7), 5973–5982.

Tariku, Y.A., 2015. Comparison of GPS-TEC with IRI-2012 TEC over African equatorial and low latitude regions during the period of 2012–2013. Adv. Space Res. 56 (8), 1677–1685.

Tariq, M.A., Shah, M., Ulukavak, M., Iqbal, T., 2019. Comparison of TEC from GPS and IRI-2016 model over different regions of Pakistan during 2015–2017. Adv. Space Res. 64 (3), 707–718.